Adv. Manuf.
https://doi.org/10.1007/s40436-023-00471-z

Research on feed-pulse collaborative control method in micro-electrical discharge machining

Qiang Gao[1,2] · Ya-Ou Zhang[1,2] · Xue-Cheng Xi[1,2] · Yuan-Ding Wang[3] · Xiao-Fei Chen[3] · Wan-Sheng Zhao[1,2]

Received: 3 April 2023 / Revised: 1 June 2023 / Accepted: 31 October 2023

Abstract Reducing the short-circuit rate and increasing the effective discharge rate are important targets for improving the servo control effect of micro-electrical discharge machining (micro-EDM), as these two indicators are closely related to the machining efficiency and quality. In this study, a feed-pulse collaborative control (FPCC) method is proposed for micro-EDM based on two dimensions (space and time). In the spatial dimension, a feed control strategy with a discharge holding process is adopted. Meanwhile, in the time dimension, a forward-looking pulse control strategy is adopted, in which the pulse interval is adjusted based on a sequence analysis of feed commands and discharge states. Process experiments are carried out to determine the key parameters used in this method, including the discharge holding threshold and pulse interval adjustment value ($T_{\mathrm{off}_{\mathrm{adj}}}$). The feed smoothness and discharge sufficiency analyses of the experimental results show that compared to the traditional double threshold average voltage method, the FPCC method reduces the number of long-distance retreats by 64% and improves the effective discharge time by 40%.

Keywords Micro-electrical discharge machining (micro-EDM) · Electrode feed control · Discharge pulse control · Machining surface quality

✉ Ya-Ou Zhang
yaou_zhang@sjtu.edu.cn

[1] School of Mechanical Engineering, Shanghai Jiao Tong University, Shanghai 200240, People's Republic of China

[2] State Key Laboratory of Mechanical System and Vibration, Shanghai 200240, People's Republic of China

[3] Shanghai Institute of Space Propulsion, Shanghai 201112, People's Republic of China

1 Introduction

Micro-electric discharge machining (micro-EDM) is widely used in the manufacture of micro-holes and micro-cavities, such as in the fuel injectors of automobiles and flow channels of aero-engines. In recent years, new requirements for micro-EDM, including a better surface quality and higher aspect ratio, have been put forward owing to developments in aerospace, mold manufacturing, and other industrial fields. For improving the machining ability of the micro-EDM technology, in addition to using auxiliary methods such as adding an ultrasonic vibration to a feed spindle [1], it is more crucial to improve the servo control effect of the machining control system itself. This is because the machining control strategy has a direct impact on the effective discharge rate and short-circuit rate of a machining process, which are closely related to the machining efficiency and quality [2–4]. Current research on the machining control systems of micro-EDM mainly focuses on two aspects: feed control (FC) and pulse control (PC), as shown in Fig. 1. FC refers to controlling the movement of a spindle to maintain an appropriate gap distance, whereas PC refers to controlling a pulse power supply to generate a proper discharge pulse train.

The FC methods of EDM can be roughly divided into threshold control and adaptive control. In a threshold control method, generally a gap state parameter such as the gap voltage or discharge rate is selected as a control target, and a reference threshold is predetermined for this parameter. During a machining process, the actual detected gap state is compared with the reference threshold; then, the spindle is controlled to feed or retreat accordingly. A typical threshold control method is the average voltage method [5, 6]. In contrast, the adaptive control method generally refers to adaptively or intelligently controlling the electrode feeding

Published online: 06 January 2024

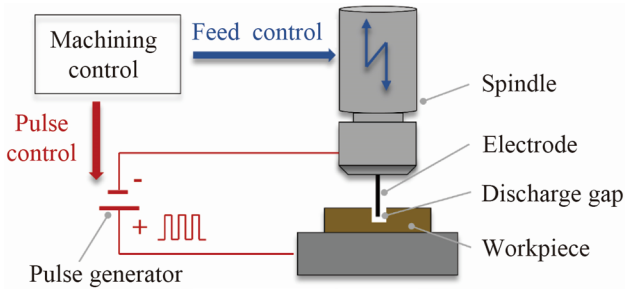

Fig. 1 Schematic diagram of feed control and pulse control in micro-EDM

process without manually setting thresholds. For example, Zhou et al. [7, 8] created a time-varied linear model for an EDM process to realize a closed-loop FC. The control law established the relationship between the gap servo-voltage and machining state, and was able to adaptively adjust the controller parameters. Zhang et al. [9] proposed a two-stage servo feed controller for micro-EDM based on the type-2 fuzzy set theory. The first stage was for detecting the discharge state and the second stage was used to obtain an appropriate feeding speed. These FC methods were designed for different machining requirements, but their successful implementations all prove that a suitable gap distance and sufficient holding time are the prerequisites for a high-frequency discharge process. This is a practical basis for the FC strategy proposed in this study.

The pulse power supply and its control strategy comprise another key technology of EDM systems. In micro-EDM, a resistor-capacitor (RC)-type pulse generator is generally used for the pulse power, because it is easier to produce a very small energy than with a transistor-type generator [10, 11]. However, by depending solely on the gap state, the discharge timing of the RC-type pulse generator is not controllable, making it difficult to immediately cut off abnormal discharges [12, 13]. Therefore, a controllable RC-type pulse generator is proposed. It is developed by adding several metal-oxide-semiconductor field-effect transistors (MOSFETs) to an original RC-type circuit. This controllable RC-type power can generate a desired pulse train according to artificially set pulse parameters, such as the pulse on-time (T_{on}) and pulse interval (T_{off}). Generally, these parameters are predetermined and are not changed during machining. In recent years, the real-time adjustment of pulse parameters has been further studied [14]. For micro-wire-EDM, Yan and Chien [15] proposed a pulse interval regulating strategy based on identified gap states. When abnormal machining states such as arc discharges occurred, the pulse interval was extended to allow sufficient time for the debris to be flushed out. These studies suggest that appropriate PC is necessary during a discharge process.

Existing research studies on servo control strategies for micro-EDM generally focus on only one aspect of FC or PC. In fact, these two aspects are not completely independent. A good cooperation between the gap distance control and pulse train generation is an important requirement for a stable machining process [16]. Han et al. [17] developed a transistor-type iso-pulse generator for micro-EDM and new FC system using an ignition delay time to monitor the gap distance. By integrating the pulse generator with the FC system, they obtained a removal rate approximately 24 times higher than that of a conventional RC-type pulse generator with a constant feed rate. Fu et al. [18] developed a new piezoelectric self-adaptive micro-EDM method. The piezoelectric actuator was not only used to drive the electrode for feeding, but also acted as an equivalent capacitor in an RC-type pulse generator. In this way, a servo control system is easy to implement and micro-EDM with a micro-energy at a low open voltage can be achieved. These studies indicate that substantial improvements in machining effects result from a good cooperation between pulse generation and FC.

In this study, to improve the effective discharge rate and reduce the short-circuit rate during machining, a feed-pulse collaborative control (FPCC) method is proposed for a micro-EDM process. The FPCC method realizes the machining control from the two dimensions of space and time, respectively. In the spatial dimension, an FC strategy based on effective discharge times is adopted, in which an appropriate discharge holding threshold (DHT) is determined to increase the discharge probability. Meanwhile, in the time dimension, a forward-looking PC strategy is proposed based on a feed and discharge sequence analysis. The pulse interval is adaptively adjusted according to a predicted gap state to reduce the short-circuit rate. To realize the FPCC method, a collaborative control system integrating three modules (power generator control, discharge state identification, and electrode feed drive) is designed.

2 Methodology

2.1 Feed-pulse collaborative control system

Figure 2 shows the topology of the FPCC system. The field programmable gate array (FPGA) is the core unit of the system. It generates drive signals for the MOSFETs of an RC-type pulse power, acquires voltages from the discharge gap, and

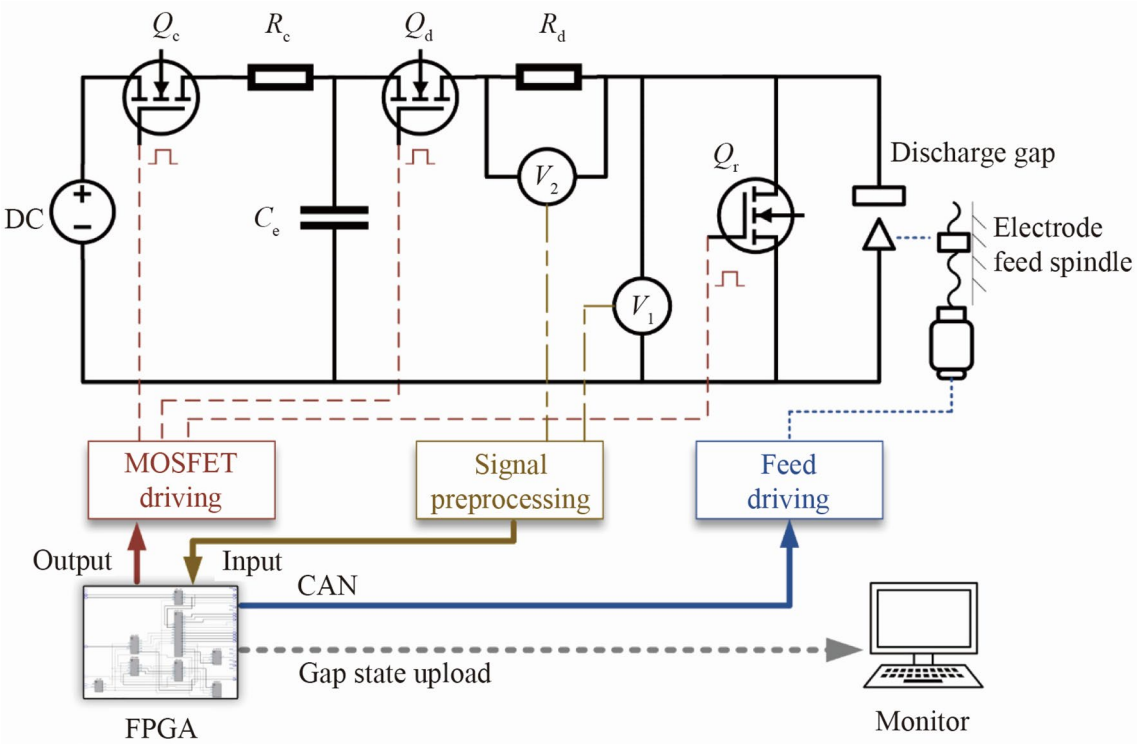

Fig. 2 Topology of the feed-pulse collaborative control system

controls the movement of an electrode feed spindle. In the RC-type pulse power, C_e is an energy storage capacitor and R_c is a current limiting resistor. Q_c and Q_d are the MOSFETs used to control the charging and discharging process of C_e, respectively. By controlling the turn-on times of Q_c and Q_d, the pulse interval ($T_{off_{adj}}$) and pulse on-time (T_{on}) of the discharge pulses can be adjusted. Q_r is used to cut off the path between C_e and the discharge gap. It is turned on at an appropriate time to release the gap energy. The two voltage probes V_1 and V_2 are designed for gap information collection. V_1 is used to detect the voltage from the discharge gap (gap voltage), whereas V_2 is set to acquire the R_d voltage for indirectly measuring the gap current. The collected V_1 and V_2 signals are analyzed by the FPGA, and then feed driving commands are sent to the spindle through a controller area network bus.

The FPCC apparatus consists of an FPGA unit, a group of MOSFETs, an RC circuit, and two voltage probes, as shown in Fig. 3a. The micro-EDM machine tool used for experiments is shown in Fig. 3b. The spindle module is used to realize the clamping, rotation, and feeding of a micro-electrode, whereas the *X*-axis and *Y*-axis are adopted to implement a scanning movement for plane milling. The numerical control system of the EDM machine is independently developed by the in-house team and hence the communication between the FPGA and the machine tool can be established conveniently through adding several programs to the control system.

2.2 Discharge state identification based on single-pulse detection

In EDM, an accurate discharge state identification is the prerequisite for effective servo control. A common identification method is to judge the discharge state based on the collected gap voltage and current within a total servo cycle T_s [19]. However, usually, a large number of discharge pulses exist within one servo cycle. The collected gap signals may be mixed with the information of a non-discharge phase, such as pulse interval stage, and may also contain noise components [20]. Therefore, it is difficult to accurately locate effective discharge pulses, which may cause misjudgment of a discharge state. In this study, with the help of the collaborative control system shown in Fig. 1, the starting and ending moments of each pulse are precisely known. Therefore, the discharge state identification can be performed based on single-pulse detection.

As shown in Fig. 4, the driver signal of Q_d accurately reflects the T_{on} and T_{off} stages of each pulse cycle. Considering that a discharge only occurs at the T_{on} stage, the voltage sampling can be performed only if Q_d is turned on. When a falling edge of V_1 and peak value of V_2 are detected in a T_{on} stage, the pulse is judged as a normal discharge pulse [21]. In contrast,

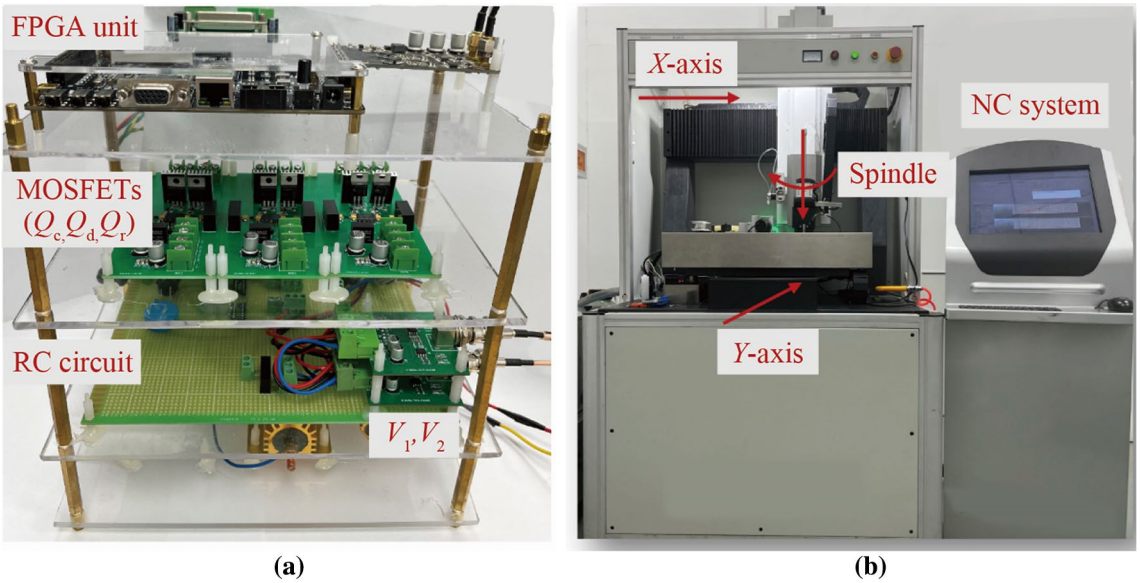

Fig. 3 Experimental system **a** FPCC apparatus and **b** micro-EDM machine tool

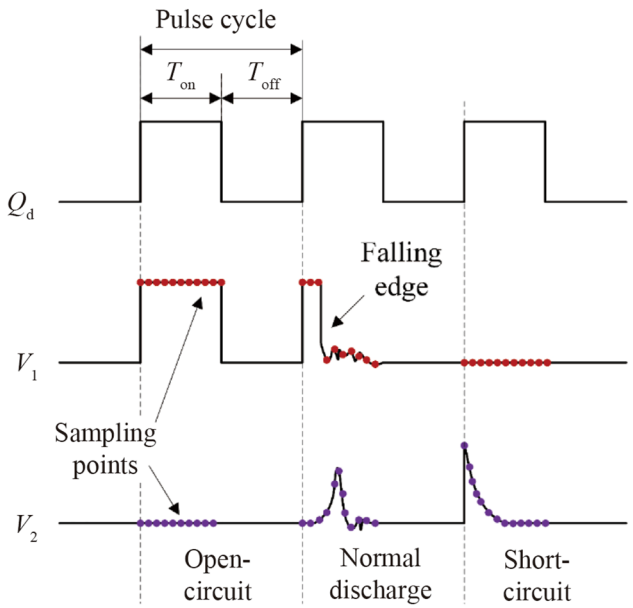

Fig. 4 Drive signal of Q_d and voltage waveforms of different pulses

an open-circuit pulse and short-circuit pulse respectively correspond to V_1 maintaining at a large value or V_2 showing an exponential decline process.

2.3 Feed control strategy based on effective discharge times

The FC is performed based on the statistical results of the discharge times within a servo cycle. As shown in Fig. 5, during a servo cycle, each pulse is identified and counted based on the single-pulse detection described in Sect. 2.2. $N_{dis}(k)$, $N_{op}(k)$, and $N_{st}(k)$ represent the number of normal discharge pulses, open-circuit pulses, and short-circuit pulses within the kth servo cycle, respectively. $N_{tot}(k)$ is the total number of all pulses. When a servo cycle ends, the gap state identification and corresponding FC are carried out. If $N_{dis}(k) \geq$ DHT is satisfied, the current cycle is determined as in an effective discharge state and the electrode is controlled to hold at the current position without movement. On the contrary, a large value of $N_{op}(k)/N_{tot}(k)$ or $N_{st}(k)/N_{tot}(k)$ means that the gap lies in an open-circuit state or short-circuit state, and accordingly, the feed or retreat movements of an electrode should be carried out. In addition, if none of the above conditions are satisfied, it may indicate that the gap is in a possible abnormal discharge state. At this time, only Q_r is turned on to temporarily close the pulse output. Nevertheless, it should be pointed out that under the control flow shown in Fig. 5, the operation of turning off the pulse output is only triggered in a few cases. For most actual abnormal discharge states, the retreat movement of the electrode is carried out.

The specific control flow of the electrode feeding is as follows. The control system executes the operations shown in Fig. 5 cyclically with a servo cycle $T_s = 100$ ms. In a servo cycle, each discharge pulse is judged and counted. Depending on whether the pulse is judged as a normal discharge pulse, open-circuit pulse, or a short-circuit pulse, one of $N_{dis}(k)$, $N_{op}(k)$, or $N_{st}(k)$ is correspondingly increased by 1. When one servo cycle ends, that is, when the time of a single pulse multiplied by the total number of pulses is greater than T_s, $N_{tot}(k)\times(T_{on}+T_{off})>T_s$, the gap state identification and electrode FC are performed. This process is carried out

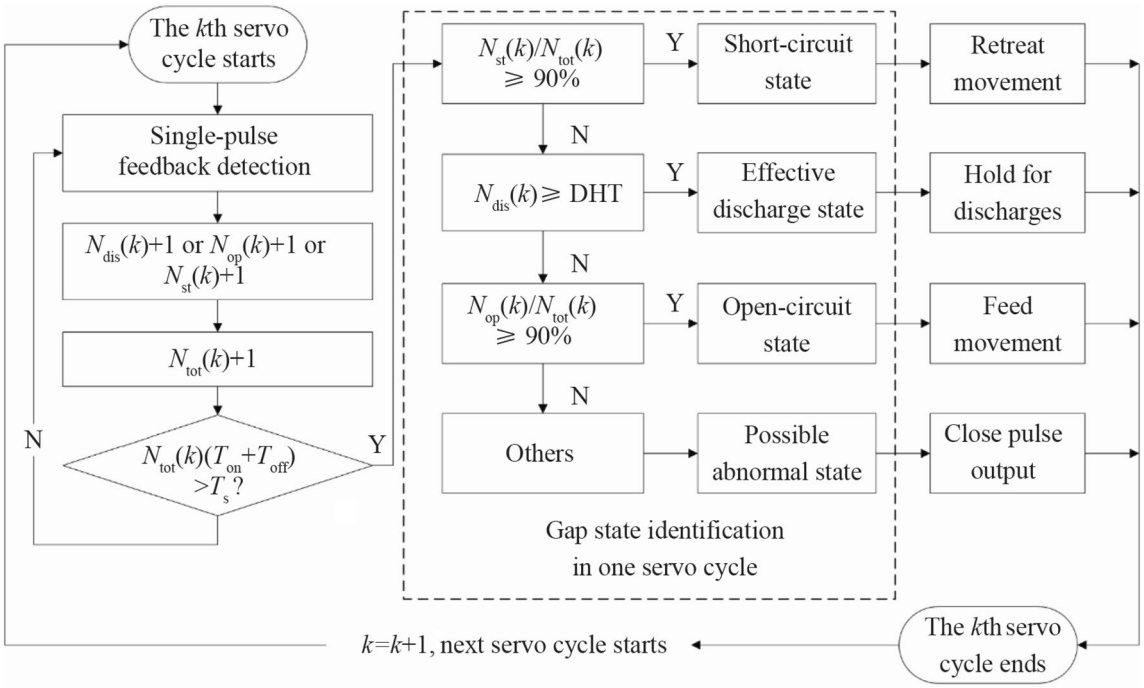

Fig. 5 Flow chart of feed control strategy

in the following order. First, the short-circuit state is identified. If the proportion of short-circuit pulses, $N_{st}(k)/N_{tot}(k)$, is not less than 90%, the electrode will be controlled to retreat immediately and this servo cycle will be ended. On the contrary, if the result of $N_{st}(k)/N_{tot}(k)$ does not meet the conditions of the short-circuit state, the gap state will continue to be identified through the number of normal discharge pulses, $N_{dis}(k)$. If $N_{dis}(k)$ is greater than DHT, the gap state will be identified as an effective discharge state. At this time, the electrode will be controlled to hold at current position, that is, it will neither feed nor retreat, so as to maintain a stable discharge gap. By analogy, if the condition of $N_{dis}(k) \geq$ DHT is not satisfied, the control system will continue to execute an open-circuit state judgment and carry out a corresponding electrode FC. Within a single servo cycle, the feed or retract distance of the electrode are both 1 um. Through this strategy, the control system can accurately locate the moment when an effective discharge state occurs according to the statistical results of the discharge pulses. The subsequent discharge holding process is conducive to maintaining a stable inter-electrode gap, so that the discharge can be fully completed.

2.4 Pulse control strategy based on sequence analysis of feed commands and discharge states

In the FC strategy proposed in Sect. 2.3, the feed command is generated only based on the state of current one servo cycle, whereas the discharge states in other historical cycles are not considered. This is to ensure a high response sensitivity for the electrode feeding process. However, the PC can be performed based on the discharge states over several consecutive cycles [22]. This is because the discharge state information of multiple cycles can be regarded as a time sequence data, which usually shows a tendency and can be used to predict the future machining state. For example, if the short-circuit state occurs frequently in the historical discharge states and the electrode happens to be controlled to feed at the current cycle, a high probability exists that a short-circuit will occur again in the next cycle. In this study, based on the sequence analysis of the feed commands and discharge states, a forward-looking PC strategy is proposed for temporarily adjusting the pulse interval at an appropriate moment. When a short-circuit state is predicted to occur, the pulse interval will be extended from the predetermined T_{off} to $T_{off_{adj}}$, so as to provide sufficient time for the recovery of the discharge gap and avoid a possible abnormal discharge state. The specific PC strategy is as follows.

For the k_{th} servo cycle, the feed command sequence $\boldsymbol{F}_d$ and short-circuit ratio sequence $\boldsymbol{R}_{st}$ composed of several historical data can be expressed

$$\boldsymbol{F}_d = [f_d(k-m), f_d(k-m+1), f_d(k-m+2), \cdots, f_d(k)], \quad (1)$$

$$\boldsymbol{R}_{\mathrm{st}} = [r_{\mathrm{st}}(k-n), r_{\mathrm{st}}(k-n+1), r_{\mathrm{st}}(k-n+2), \cdots, r_{\mathrm{st}}(k)]. \tag{2}$$

In the above, $f_{\mathrm{d}}(k)$ represents the feed value of the kth servo cycle

$$f_{\mathrm{d}}(k) = \begin{cases} 1, \text{ feed}, \\ 0, \text{ hold}, \\ -1, \text{ retreat}. \end{cases} \tag{3}$$

$r_{\mathrm{st}}(k)$ is the short-circuit ratio of the kth servo cycle and is calculated

$$r_{\mathrm{st}}(k) = N_{\mathrm{st}}(k)/N_{\mathrm{tot}}(k). \tag{4}$$

$f_{\mathrm{d}}\ (k-m)$ and $r_{\mathrm{st}}\ (k-n)$ represent the feed value and short-circuit ratio of the previous mth and nth cycle, respectively. Based on the $\boldsymbol{F}_{\mathrm{d}}$ sequence and $\boldsymbol{R}_{\mathrm{st}}$ sequence, $\bar{f}_{\mathrm{d}}(k)$ and $\bar{r}_{\mathrm{st}}(k)$, used to characterize the historical feeding condition and short-circuit situation at the k_{th} servo cycle, respectively, are proposed

$$\bar{f}_{\mathrm{d}}(k)=(1-\omega)\sum_{m=0}^{M}\omega^{m} f_{\mathrm{d}}(k-m), \tag{5}$$

$$\bar{r}_{\mathrm{st}}(k) = \frac{1}{N}\sum_{n=0}^{N} r_{\mathrm{st}}(k-n). \tag{6}$$

It is believed that the feed command data closer to the current kth servo cycle have a greater impact on the gap state. Therefore, $\bar{f}_{\mathrm{d}}(k)$ is obtained by taking an exponentially weighted average of the $\boldsymbol{F}_{\mathrm{d}}$ data and ω is a weighting coefficient. In contrast, by calculating the arithmetic mean of the $\boldsymbol{R}_{\mathrm{st}}$ data, $\bar{r}_{\mathrm{st}}(k)$ is used to characterize the deterioration of the machining state over a period of time.

As indicated by Eq. (7), in the kth servo cycle, if $\bar{f}_{\mathrm{d}}(k)$ and $\bar{r}_{\mathrm{st}}(k)$ are greater than the prediction thresholds H_{d} and H_{st}, respectively, it is considered that a short-circuit state may occur in the next several cycles. At this moment, the pulse interval adjustment will be performed.

$$\begin{cases} \left|\bar{f}_{\mathrm{d}}(k)\right| > H_{\mathrm{d}}, \\ \bar{r}_{\mathrm{st}} > H_{\mathrm{st}}\,. \end{cases} \tag{7}$$

3 Experimental procedures

3.1 Determination of discharge holding threshold (DHT)

In the FC strategy proposed in Sect. 2.3, the DHT is a very important parameter because it distinguishes between two types of feed commands: discharge holding or continuous feeding. To study the effect of the DHT on a machining process, drilling experiments with different DHT values were carried out. Table 1 lists the experimental conditions. Corresponding to the control system shown in Fig. 2, the open-circuit voltage and discharge capacitance in the table refer to the voltage of the power supply DC and capacitance of C_{e}, respectively. The setting of T_{on} and T_{off} is realized by controlling the turn-on times of Q_{d} and Q_{c}.

Table 1 Conditions used in DHT determination experiments

Parameters	Conditions
Open-circuit voltage/V	80
Discharge capacity/pF	4 700
Pulse on-time (T_{on})/μs	4
Pulse interval (T_{off})/μs	6
Workpiece material	Stainless steel
Electrode material	Tungsten carbide (–)
Electrode diameter/μm	200
Dielectric	Deionized water
Spindle speed/(r.min^{-1})	2 000
Drilling depth/μm	1 000 (Blind hole)
DHT	10, 25, 50, 100, 150, 200–1 000

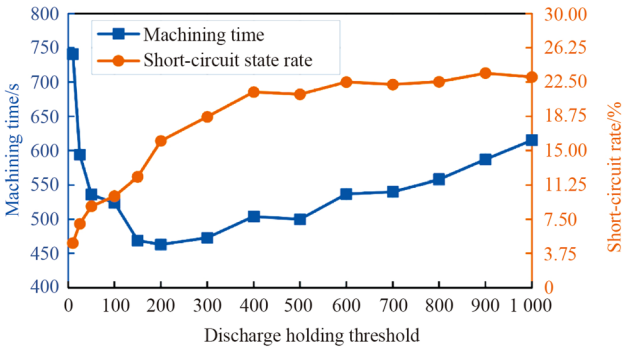

Fig. 6 Machining time and short-circuit rate under different DHT values

The experimental results shown in Fig. 6 illustrate the machining times and short-circuit rates under different DHT values (here, the short-circuit rate refers to the ratio of the number of short-circuit cycles to the number of total servo cycles). It can be seen that with the increase of DHT, the machining time presents a trend of first decreasing and then increasing. This can be explained by the relationship between the DHT and identified gap state in a servo cycle. When a small DHT is used, the gap state is more likely to be identified as a discharge holding state, and hence the feeding process is relatively slow at this time. For example, setting DHT = 1 means that as long as one discharge occurs, the electrode will be controlled to wait for discharges instead of

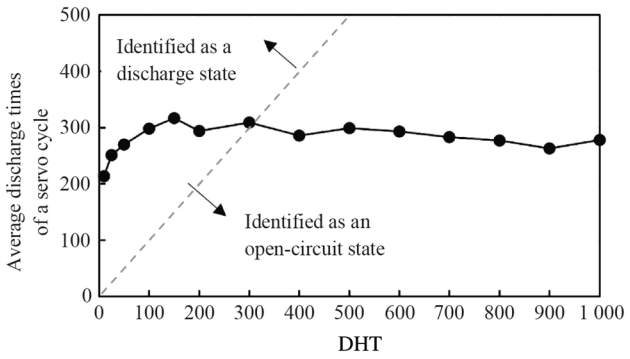

Fig. 7 Average discharge time $\overline{N}_{dis}$ under different DHT values

feeding, which will result in a long machining time. Therefore, within a certain range, increasing the DHT can shorten the machining time. However, when an excessively large DHT is used, the condition of $N_{dis}(k) \geq$ DHT is not easily satisfied. At this time, a great probability exists that the gap state is identified as an open-circuit state and hence the electrode is in a consecutive feeding process. The fast feed of the electrode causes a large number of short-circuits, thereby prolonging the machining time. This analysis can be verified by the short-circuit rate curve shown in Fig. 6, which increases continuously with the increase of the DHT.

The reason for the above phenomenon can be further explained based on the effective discharge times during a feeding process. For the experiments under different DHT values, the average discharge times of a servo cycle $\overline{N}_{dis}$ is calculated

$$\overline{N}_{dis} = \frac{\sum_{k=1}^{K} N_{dis}(k)}{K}, \tag{8}$$

where K is the total number of servo cycles in a drilling process. The results are shown in Fig. 7. A dotted line at the position where $\overline{N}_{dis}$= DHT divides the chart into two regions: on the upper side of the dotted line, $\overline{N}_{dis}$> DHT. At this time, for most of the servo cycles, the gap state tends to be identified as an effective discharge state. Conversely, on the lower side of the dotted line, $\overline{N}_{dis}$< DHT is satisfied, and hence the gap state tends to be identified as an open-circuit state during most of the servo cycles. In this region, even if DHT is increased, $\overline{N}_{dis}$ cannot be further improved. This indicates that the maximum discharge times that can be achieved are basically fixed when the pulse energy is kept unchanged. In this case, increasing the DHT will only cause an increase in the short-circuit rate.

In conclusion, the DHT can be determined according to the "$\overline{N}_{dis}$-DHT" curve. Firstly, it should be selected on the upper side of the dotted line, so that the discharge holding process can take effect and the short-circuits caused by excessive feeding can be avoided. On this basis, the DHT should be determined as an appropriate value to fully utilize the maximum discharge capacity of the power supply. In other words, its value should ensure the maximum average discharge times by as much as possible. For example, in the situation shown in Fig. 7, an appropriate range of the DHT may be [100, 300]. In this range, the most suitable value should be 150, as the average discharge times at this time is the largest.

3.2 Study on pulse interval adjustment strategy

The experiments for studying the pulse interval adjustment strategy were carried out according to the conditions shown in Table 1. During these experiments, the parameter DHT was fixed at 200. First, the experiment without pulse interval adjustment was performed. $\overline{f}_d(k)$ and $\overline{r}_{st}(k)$ as calculated during a machining process were recorded in real time, as shown in Fig. 8. According to the changing trend of $\overline{f}_d(k)$ and $\overline{r}_{st}(k)$, the machining process can be divided into three stages: the touch stage, stable machining stage, and deep machining stage. When the electrode initially touches the workpiece, a stable discharge state has not yet formed, so $\overline{f}_d(k)$ exhibits evident oscillations. After a period of time, the machining process gradually enters a stable stage.$\overline{f}_d(k)$ is basically maintained in a non-negative range, indicating that the electrode is in a stable feeding state without frequent retreat movements. At this time, $\overline{r}_{st}(k)$ also remains at a low level. However, with an increase in the drilling depth, the expelling of debris and introduction of new fluid become increasingly difficult. The large oscillation of $\overline{f}_d(k)$ indicates the frequent "feed and retreat" movements of the electrode, and $\overline{r}_{st}(k)$ also increases substantially. In this case, the probability of abnormal discharges is very high and the machined surface may be ablated. Therefore, in the unstable machining stage, and especially in the deep machining stage, it is necessary to appropriately increase the pulse interval to leave sufficient time for the recovery of the discharge gap [23]. As for the timing of pulse interval adjustment, it can be determined by analyzing $\overline{f}_d(k)$ and $\overline{r}_{st}(k)$, as already clarified by Eq. (7). Moreover, the prediction thresholds H_d and H_{st} in Eq. (7) can be determined according to the main distribution ranges of $\overline{f}_d(k)$ and $\overline{r}_{st}(k)$ in the stable machining stage, as shown in Fig. 8.

To determine an appropriate pulse interval adjustment value $T_{off_{adj}}$, experiments with different values of $T_{off_{adj}}$ were carried out. The recorded short-circuit rates of the different experiments are shown in Fig. 9. In all experiments, the preset pulse interval T_{off} is 6 μs. The first data point in the figure shows the initial short-circuit rate of the experiment without the pulse interval adjustment, whereas the next three data points are the short-circuit rates when the pulse interval is expanded to two

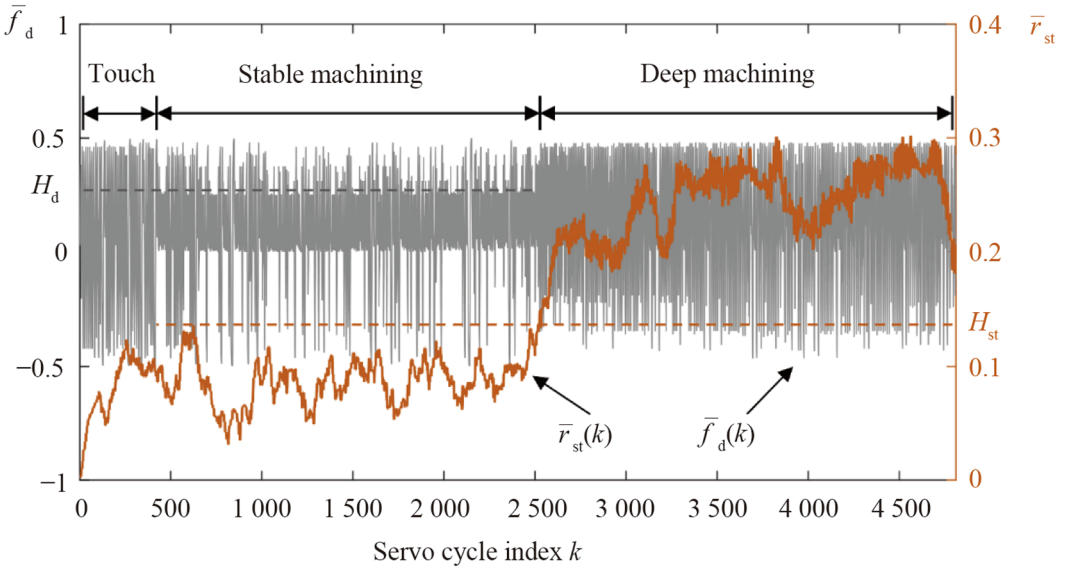

Fig. 8 $\bar{f}_d(k)$ and $\bar{r}_{st}(k)$ calculated according to Eqs. (5) and (6) during a drilling process

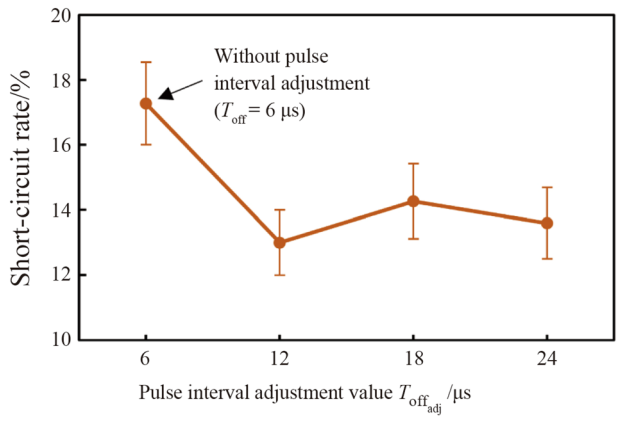

Fig. 9 Short-circuit rate under different $T_{off_{adj}}$

times, three times, and four times the original value at an appropriate time. It can be found that the adoption of the PC strategy significantly reduces the short-circuit rate of a machining process. In other words, prolonging the pulse interval before a predicted poor machining state can reduce the probability of abnormal discharges. Another finding is that the short-circuit rate does not decrease further with the increase of $T_{off_{adj}}$. This may be owing to the fact that the existence of large pulse intervals takes up an excessive amount of time, reducing the number of total pulses in a fixed servo cycle T_s. As a result, the effective discharge rate is reduced, which in turn affects the normal material removal process. Therefore, $T_{off_{adj}}$ cannot be excessively large. In this study, $T_{off_{adj}}$ is set to be twice the preset pulse interval T_{off}.

4 Verifications

4.1 Comparative experiment design

To verify the effectiveness of the FPCC method, comparative experiments which with the FPCC method and traditional average voltage methods were designed and carried out. The machining experiments using the average voltage methods were still conducted on the experimental system shown in Fig. 3, and the servo cycle was $T_s = 100$ ms. Figure 10 shows the main control flow of the average voltage methods. Instead of counting discharge times, the FPGA acquires the gap voltage at each sampling point at a high frequency ($1/T_c$, $T_c = 2$ μs). When a servo cycle ends, the average gap voltage of this cycle U_a is calculated and used for the FC. According to the number of voltage reference thresholds, the subsequent control process can be divided into two methods: single threshold average voltage (1TAV) method and double threshold average voltage (2TAV) method. The 1TAV method means that the average voltage is only compared with one reference voltage U_r. When $U_a \geq U_r$, the electrode is controlled to feed, otherwise it is controlled to retreat. In contrast, in the 2TAV method, two voltage thresholds exist, i.e., U_{r1} and U_{r2}. In addition to feed and retreat

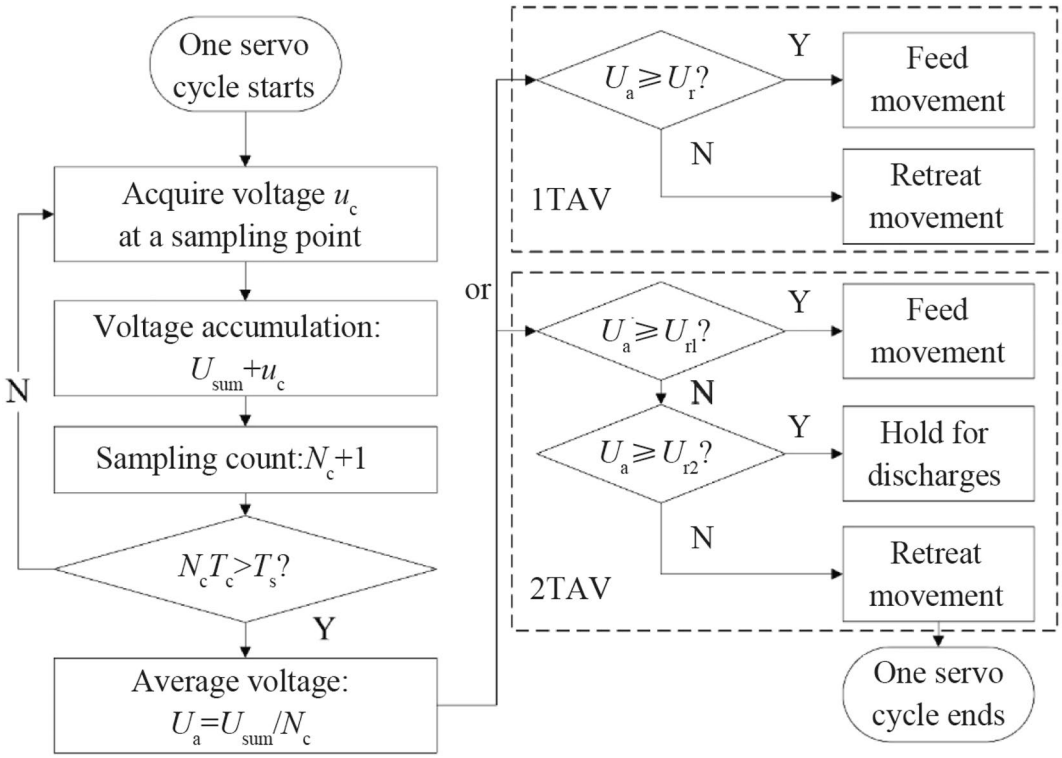

Fig. 10 Flow chart of two average voltage methods

Table 2 Parameters used in comparative experiments

Method	Parameter 1 (P1)	Parameter 2 (P2)
FC	DHT = 200	DHT = 250
FPCC	DHT = 200, $T_{off_{adj}}$ = 12 μs	DHT = 250, $T_{off_{adj}}$ = 12 μs
1TAV	U_r = 20 V	U_r = 25 V
2TAV	U_{r1} = 30 V, U_{r2} = 10 V	U_{r1} = 30 V, U_{r2} = 20 V

movements, when $U_{r1} < U_a < U_{r2}$ is satisfied, the electrode will be controlled to stop moving for discharges [24].

Table 2 lists the parameters used in the comparative experiments. FC and FPCC denote the control methods proposed in this study. FC refers to the FC method described in Sect. 2.3 without the pulse interval adjustment, whereas FPCC denotes the collaborative control method including both FC and PC. 1TAV and 2TAV are the two average voltage methods for comparison. For each method, two groups of parameters, P1 and P2, are selected for experiments, whereas the other conditions are consistent with those listed in Table 1. Sections 4.2 and 4.3 describe the results of through-hole experiments and high-aspect-ratio blind-hole drilling experiments, respectively.

4.2 Through-hole drilling experiments

In the through-hole drilling experiments, the machined workpiece is a sheet with a thickness of 1 000 μm, and the total feeding depth of the electrode is set to 1 500 μm to reduce the taper of the hole by an extra feed process. Figure 11 shows the machining time, discharge frequency, and short-circuit rate values of the experiments using the four methods under the two groups of parameters. It can be seen from Fig. 11a that the machining times of the FC and FPCC methods are shorter than those of the average voltage methods. In detail, the machining time of the FC method is shortened by 21% compared to the 1TAV method and by 12% compared to the 2TAV method. Similarly, the machining time of the FPCC method is also reduced by 17% and 8% compared with the 1TAV method and 2TAV method, respectively. The direct reason for this result can be found in Figs. 11b and c. That is, the FC and FPCC methods have a higher discharge frequency and hence the material removal rate is improved. However, in the 1TAV and 2TAV methods, the short-circuit rate is relatively larger. The frequent short-circuit retreat movements of the electrode take up a significant amount of time, thereby reducing the machining efficiency.

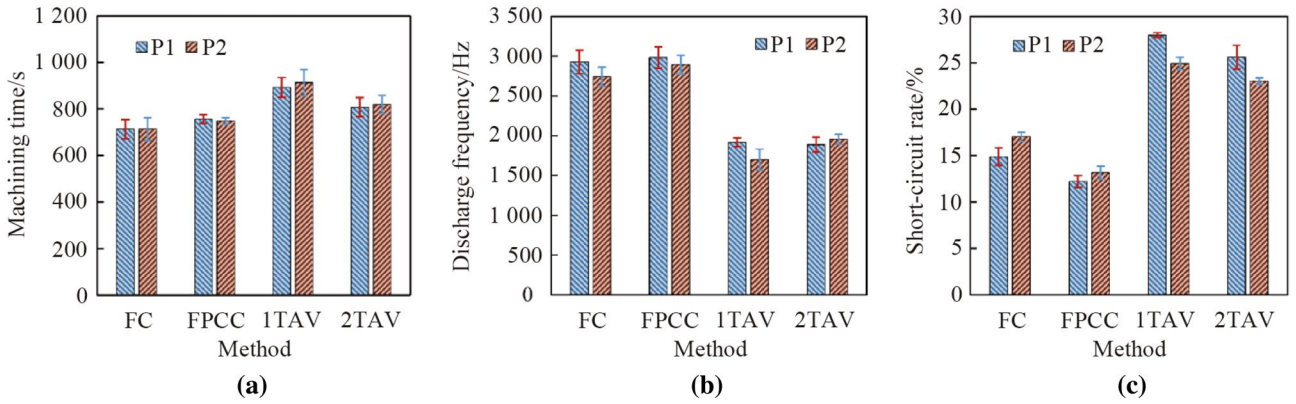

Fig. 11 Results of through-hole drilling experiments **a** machining time, **b** discharge frequency, and **c** short-circuit rate

It can also be found from Fig. 11c that compared with the FC method, the short-circuit rate of the FPCC method is further reduced by 20%. This demonstrates that the PC strategy is effective. When the gap state tends to be short-circuited, the pulse interval is appropriately increased, thereby reducing harmful discharges. In addition, the short-circuit rate of the 2TAV method is further reduced by approximately 8% compared to that of the 1TAV method. One possible reason is that the 2TAV method uses a discharge holding command similar to that used in the FC or FPCC method. This discharge holding process makes the electrode in an intermittent state rather than in a consecutive feeding state, improving the discharge probability and avoiding the short-circuits caused by an excessive feeding process.

4.3 High-aspect-ratio blind-hole drilling experiments

In high-aspect-ratio blind-hole drilling experiments, the thickness of the workpiece is large enough for blind-hole drilling and the total feeding depth of the electrode is set to 2 200 μm. Considering the diameter of an electrode and size of a discharge gap, the aspect ratio of the drilling hole is approximately in the range of 9–10, which can be regarded as a high-aspect-ratio drilling in micro-EDM. Figure 12 shows the typical morphologies of the deep blind holes machined by the FPCC, 1TAV, and 2TAV methods, respectively. It can be found that several over-eroded regions exist in the hole sidewalls machined using the 1TAV and 2TAV methods, whereas the sidewall machined using the FPCC method is relatively smooth. Usually, the appearance of the over-eroded regions is caused by abnormal discharges and the resulting frequent retreat movements [25]. Therefore, it can be demonstrated that compared with the average voltage methods, the FPCC method significantly reduces the short-circuit retreat movements.

Figure 12 also shows the roughness of the top, middle, and bottom regions of the three holes, which were measured using an optical profile measuring instrument, the Alicona InfiniteFocus G5. In the middle and bottom regions of the holes, the roughness order is FPCC < 2TAV < 1TAV, indicating that the surface quality machined by the FPCC method is the best. In detail, the microscopic morphologies and roughness measurement curves of the middle regions are shown in Fig. 13. It can be found that no significant differences exist in the morphologies of the single discharge craters generated using the three methods. This is because the experiments were all carried out using the same control system and the pulse power parameters were also the same. The differences in roughness in the three methods can be attributed to the differences in the crater density and crater distribution. As shown in Fig. 13, the roughness measurement curves of the FPCC and 2TAV methods have relatively smaller fluctuations, whereas that of the 1TAV method exhibits several larger peaks. This shows that the distribution of the discharge craters machined using the 1TAV method is not as uniform and dense as those of the other two methods. One possible reason is that the discharge holding strategy in the FPCC and 2TAV methods provides a sufficient time for the discharge process to complete, thereby making the material removal more effective.

5 Discussions

5.1 Feed smoothness

To further explain the reasons for the different machining results, the feed smoothness during a machining process is discussed. Figure 14a shows the "feed position-machining time" curves of the FC, FPCC, 1TAV, and 2TAV methods during a group of high-aspect-ratio blind-hole drilling experiments. In these curves, to distinguish between the effects of the FC and PC, the "pulse output close" operation in Fig. 5

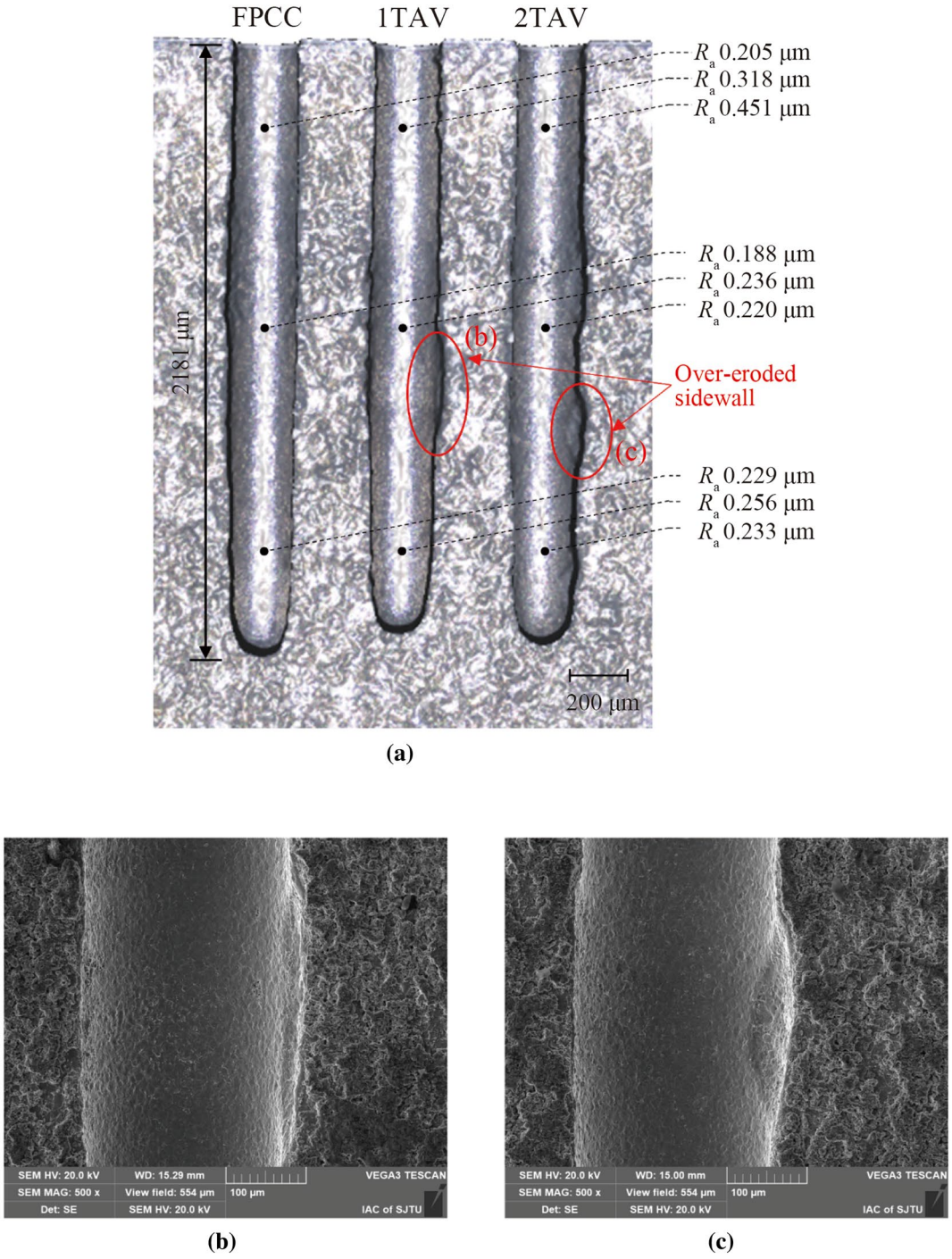

Fig. 12 Morphologies and roughness of blind holes machined by FPCC, 1TAV and 2TAV methods **a** global view of hole sidewalls, **b** SEM image of the over-eroded region in the 1TAV method, **c** SEM image of the over-eroded region in the 2TAV method

included in the FC and FPCC method is turned off. On the whole, it can be seen from Fig. 14a that the FC and FPCC methods have smoother feed curves and shorter machining times than the 1TAV and 2TAV methods. In detail, the feed curve of the FPCC method is smoother than that of the FC method, indicating that the application of the pulse interval adjustment strategy further reduces the probability of a short-circuit state. In contrast, many short-circuit retreat movements exist in the feed curves of the two average voltage methods. The morphologies of the hole sidewalls near these retreat movement positions usually exhibit excess erosion, as shown in Figs. 14b and c. This explains the reason

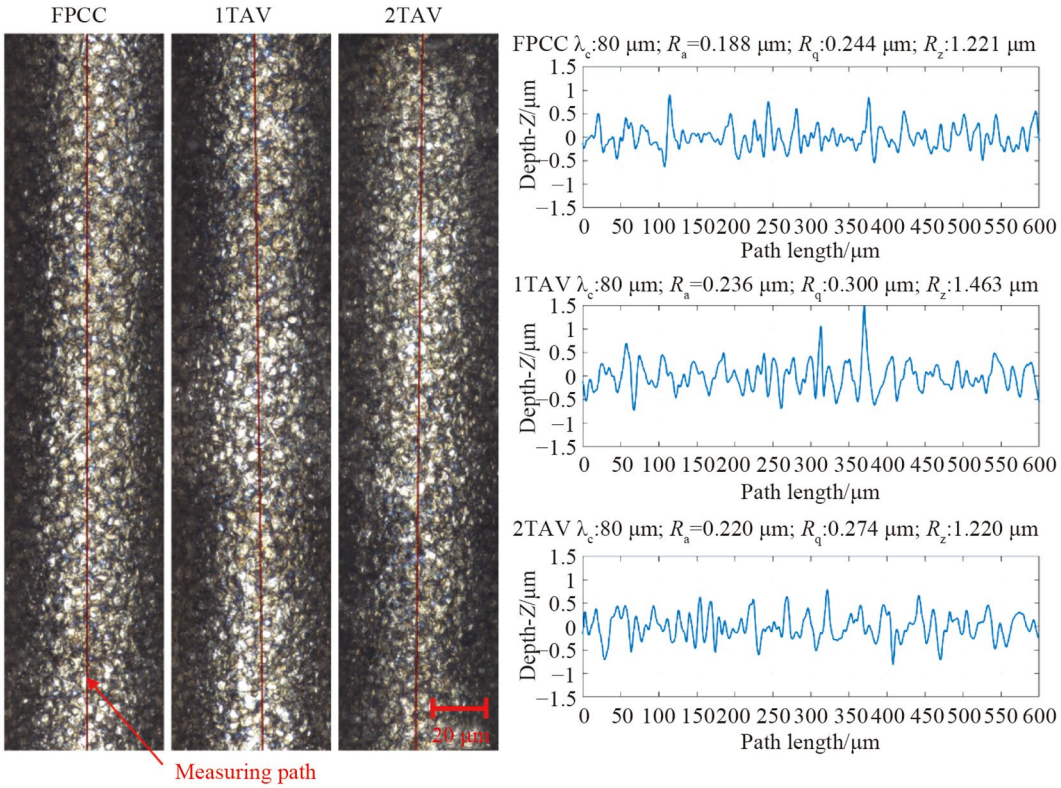

Fig. 13 Roughness measurement results of the middle-region sidewalls in Fig. 12

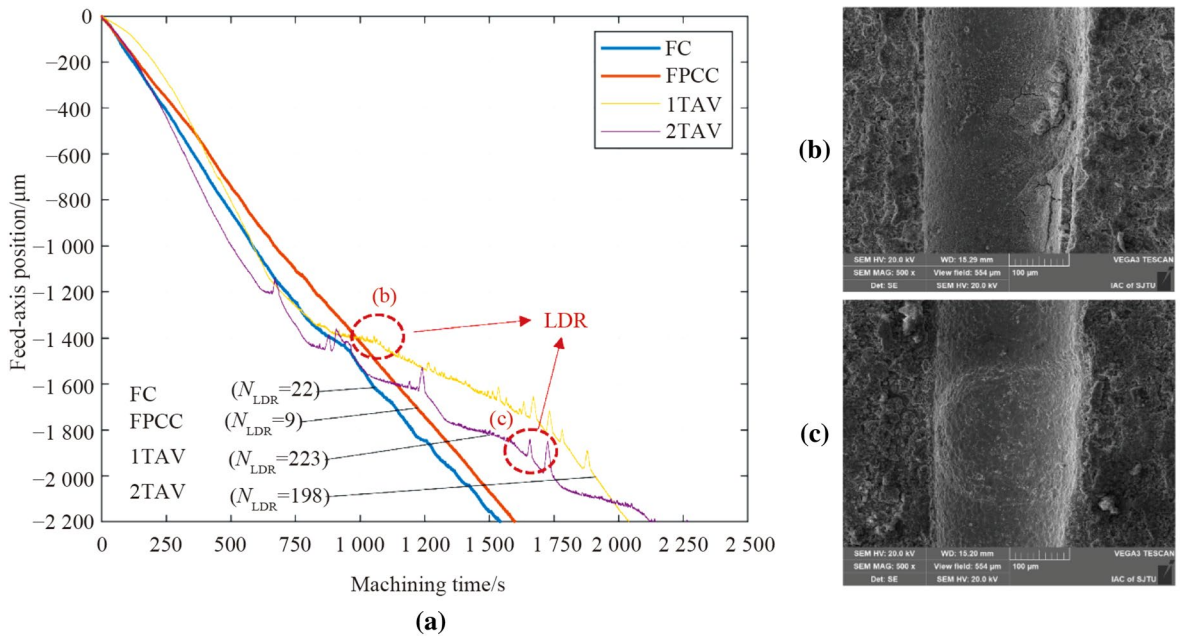

Fig. 14 Typical "feed position-machining time" curves and morphologies of the sidewalls at the LDR position **a** feed curves of the FC, FPCC, 1TAV and 2TAV methods, **b** sidewall morphology at LDR position in 1ATV method, **c** sidewall morphology at LDR in 2ATV method

for the over-eroded sidewall phenomenon that occurs in the 1TAV and 2TAV methods shown in Fig. 12.

It should be noted that the short-circuit retreat movements cannot and do not need to be completely eliminated. Even if in the FPCC machining experiments, short-circuits exist, as shown in Fig. 11c. However, it can be seen from Fig. 14 that only a small range of retreat movements appear in the FPCC method, and its feed curve is relatively smooth. This means that only the consecutive short-circuits that have a significant impact on a feed process need to be taken into account. In this study, the concept of long-distance retreat (LDR), which represents the consecutive retreat movements over a large distance, is proposed. The number of LDRs N_{LDR} during a drilling process is counted using Eq. (9).

$$N_{\mathrm{LDR}} = \sum_{j=1}^{J} \mathrm{sgn}(N_{\mathrm{cr}}(j) - H_{\mathrm{cr}}), \tag{9}$$

where $N_{\mathrm{cr}}(j)$ represents the number of retreat movements in the jth consecutive short-circuit, and H_{cr} is the threshold for judging $N_{\mathrm{cr}}(j)$ as a LDR. In this study, the length of each retreat movement during one servo cycle is 1 μm. Therefore, $H_{\mathrm{cr}} = 5$ means that when a consecutive retreat movement is larger than 5 μm, it is regarded as an LDR.

As shown in Fig. 14, the N_{LDR} values of the FC, FPCC, 1TAV, and 2TAV methods are 22, 9, 223, and 198, respectively ($H_{\mathrm{cr}} = 5$). This indicates that the feed smoothness of the FPCC method is the best and that of the 1TAV method is the worst, which explains the better machining quality and shorter machining time of the FPCC method. Furthermore, the N_{LDR} values of each method in the through-hole drilling experiments are also calculated, as shown in Fig. 15. It can be seen that the N_{LDR} of the FC method is reduced by 68% compared to that of the 1TAV method and by 29% compared to that of the 2TAV method. Moreover, the N_{LDR} of the FPCC method is also reduced by 84% compared to that of the 1TAV method and by 64% compared to that of the 2TAV method. This further verifies that the FPCC method can effectively reduce the occurrence probability of LDRs. In the FPCC method, the existence of discharge holding process avoids aggressive feed movements. At the same time, the pulse interval adjustment strategy prevents possible abnormal discharges. Thanks to an accurate identification of the discharge pulse, the holding process can be carried out timely and accurately. Meanwhile, the effectiveness of the pulse interval adjustment is also inseparable from the sequence analysis of the historical feed command data. Therefore, it can be concluded that the good cooperation between the FC and PC reduces the probability of long-distance short-circuit retreat movements, thereby making the feeding process smoother.

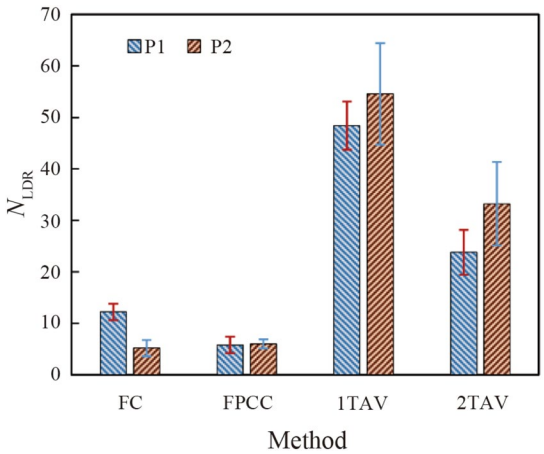

Fig. 15 N_{LDR} of different methods in through-hole drilling experiments ($H_{\mathrm{cr}} = 5$)

5.2 Discharge sufficiency

The discharge sufficiency in this study refers to the degree of effective discharge in the spatial dimension, for example, the discharge times within a certain feeding depth. The results in Fig. 11b have already shown that the FPCC method has a higher discharge frequency compared to those of the 1TAV and 2TAV methods. That is the analysis result from the time dimension. To further analyze the relationship between the discharge rate and feeding process, the effective discharge times at different feeding positions are counted and shown in Fig. 16. The region between the two dotted lines in the figure represents a 100 μm feeding length, and the black square data point in this region indicates the average discharge times of the 100 μm depth $\overline{N}_{\mathrm{dis}}^{\Delta}$.

It can be seen that the $\overline{N}_{\mathrm{dis}}^{\Delta}$ of the FPCC method is always maintained at a higher level compared to those of the other two methods. Specifically, the average discharge time in the FPCC method is 73% higher than that of the 1TAV method, and 40% higher than that of the 2TAV method. This can be explained by the effect of the discharge holding process in the FPCC method. As shown in the detailed diagram in Fig. 16, the feed curve of the FPCC method presents a step-down feature. The small horizontal line in the feed curve indicates a waiting stage of the electrode. Only when the effective discharge time is lower than the DHT will the electrode be controlled to continue feeding. This provides a sufficient time for an effective discharge process. However, in the 1TAV method, as the average gap voltage U_{a} is either larger or less than U_{r}, the electrode is always in a moving state, feed or retreat. This results in a constant change of the gap distance and is not conducive to maintaining a stable discharge state. In the 2TAV method, although a discharge holding process exists, the average discharge times are still low. This is because the discharge holding process in the 2TAV method is still determined by the gap average

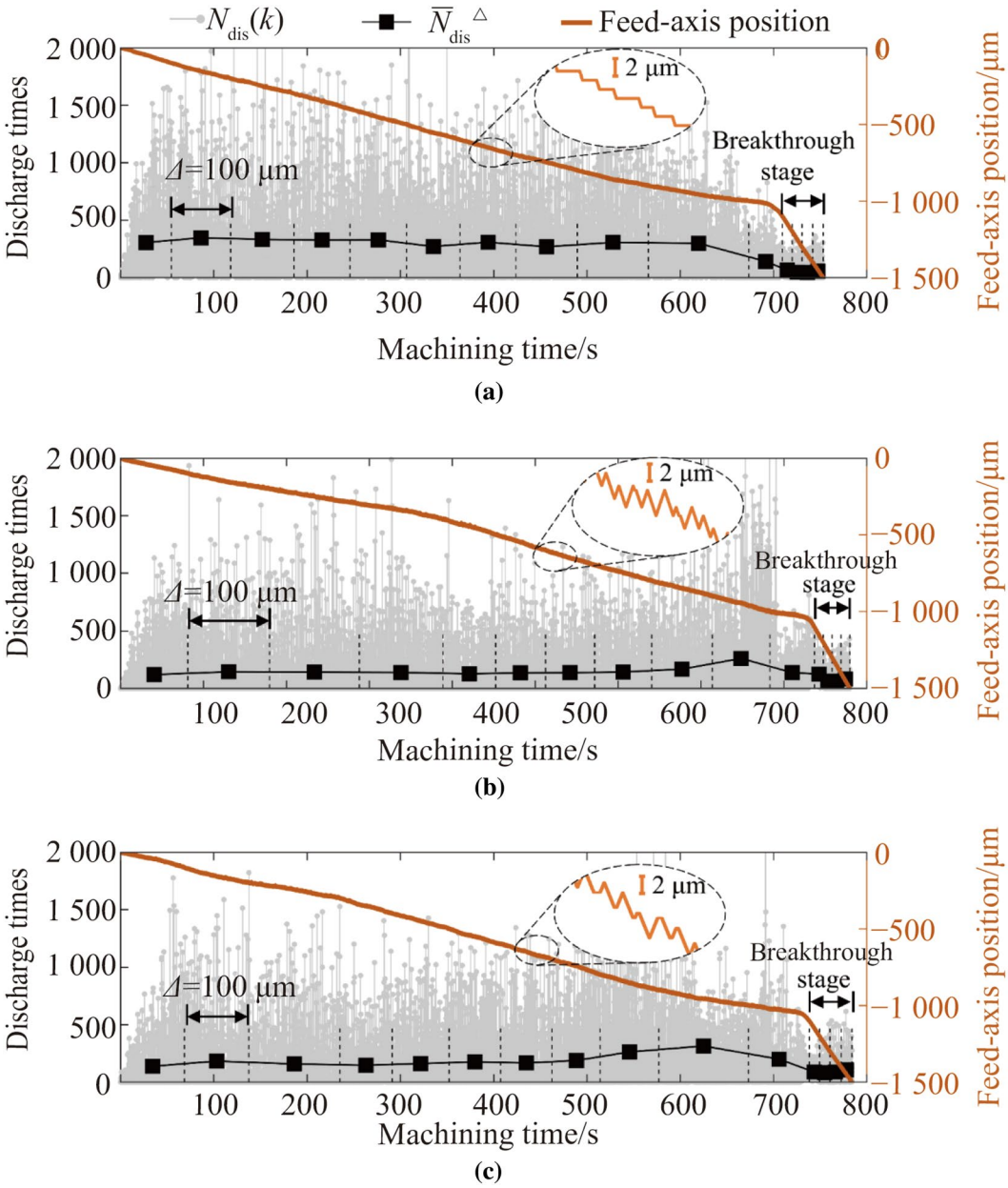

Fig. 16 Discharge times and feed curves in through-hole drilling experiments **a** using FPCC method, **b** using 1TAV method and **c** using 2TAV method

voltage U_a. The voltage averaging process causes a loss of the effective gap information and delay in the control timing. As a result, quite a few short-circuit retreat movements appear, as shown in the feed curve. In summary, it can be concluded that the discharge holding process in the FPCC method effectively increases the discharge rate and hence enables the sufficient erosion of the hole sidewall. This is one of the reasons for the better machining quality of the FPCC method.

To further study the influence of the discharge sufficiency on the machining quality, a group of milling experiments using the FPCC and 1TAV methods are carried out. The machining conditions used in the experiments are listed in Table 3. Compared with the drilling experiments, during the

Table 3 Conditions used in milling experiments

Parameters	Conditions
Open-circuit voltage/V	80
Discharge capacity/pF	4 700
Pulse on-time (T_{on})/μs	4
Pulse interval (T_{off})/μs	6
Workpiece material	Stainless steel
Electrode material	Tungsten carbide (–)
Electrode diameter/μm	200
Dielectric	Deionized water
Spindle speed/(r·min^{-1})	2 000
Feeding axis	*X*-axis and *Y*-axis linkage
Electrode compensation	No *Z*-axis compensation
Gap distance/μm	Constant at 3
DHT of FPCC method	150
U_r of 1TAV/V	25

milling experiments the feeding process of the electrode is changed to a lateral movement along the *X*-axis and *Y*-axis. Considering that the total milling length is small, no electrode wear compensation along the *Z*-axis direction is performed during machining. Specifically, the gap distance in the *Z* direction is constant at 3 μm. The milling results are shown in Fig. 17. It can be seen that the "flower" pattern machined using the FPCC method is clearer and has a better depth consistency. From the local detailed view shown in Figs. 17c and d, the groove milled using the FPCC method has a more uniform microscopic morphology than that of the 1TAV method. This indicates that the effective discharge time of the 1TAV method is relatively lower and hence the workpiece material cannot be sufficiently eroded.

The spatial distribution of effective discharge times shown in Fig. 18 can further explain the reasons for the different milling results of the two methods. In the process of plane milling, owing to a good debris-removal and fluid-introduction environment, the collected gap average voltage is usually close to the open-circuit voltage. This makes the electrode in a state of consecutive and rapid feeding when using the 1TAV method. As a result, an insufficient discharge time exists between the electrode and workpiece. The discharge rate of the 1TAV method is lower, as shown in Fig. 18b. In contrast, in the FPCC method, the FC strategy is performed based on the effective discharge times. Thanks to the collaborative control system, the starting and ending timing of each pulse are known precisely. The method of detecting the V_1 falling edge to capture a normal discharge pulse is more sensitive than that using the average voltage. When an effective discharge state is detected, the electrode will be controlled to wait until no more discharges are generated at this position. This ensures a high discharge sufficiency during a machining process. Therefore, the discharge rate of the FPCC method is larger and the spatial distribution of discharge times is more uniform, as shown in Fig. 18a.

6 Conclusions

This study presents an FPCC method for micro-EDM. A collaborative control system integrating PC, gap detection, and FC is designed. On this basis, an FC strategy with discharge holding process and forward-looking PC strategy for adjusting the pulse interval are proposed. Compared with the average voltage method, the FPCC method shortens the machining time by at least 8%, and also effectively avoids the over erosion of the hole sidewall. Below are some conclusions drawn from this study.

(i) In terms of feed smoothness, the number of LDRs in the FPCC method is reduced by 64% compared to those in the 2TAV method. Moreover, in terms of the discharge sufficiency, the FPCC method increases the effective discharge time by 40%.

(ii) The collaborative control of the electrode feed and pulse generation is effective in improving the machining efficiency and quality. Through a cooperative control mechanism, FC can be better performed because the identification of the effective discharge pulses is more accurate. Meanwhile, the PC is also more effective, as the gap state prediction can be carried out using historical feed command data.

(iii) The integrated control of the pulse output and gap detection can realize an accurate positioning of each discharge pulse. The discharge state identification based on this single-pulse detection strategy can obtain more discharge information than the traditional average voltage method.

In summary, the results of this study can be used for the control process optimization of micro-EDM, especially in some occasions where high machining quality is required. Moreover, the FPCC topology proposed in this study can also be adopted in other EDM processes, such as wire-EDM.

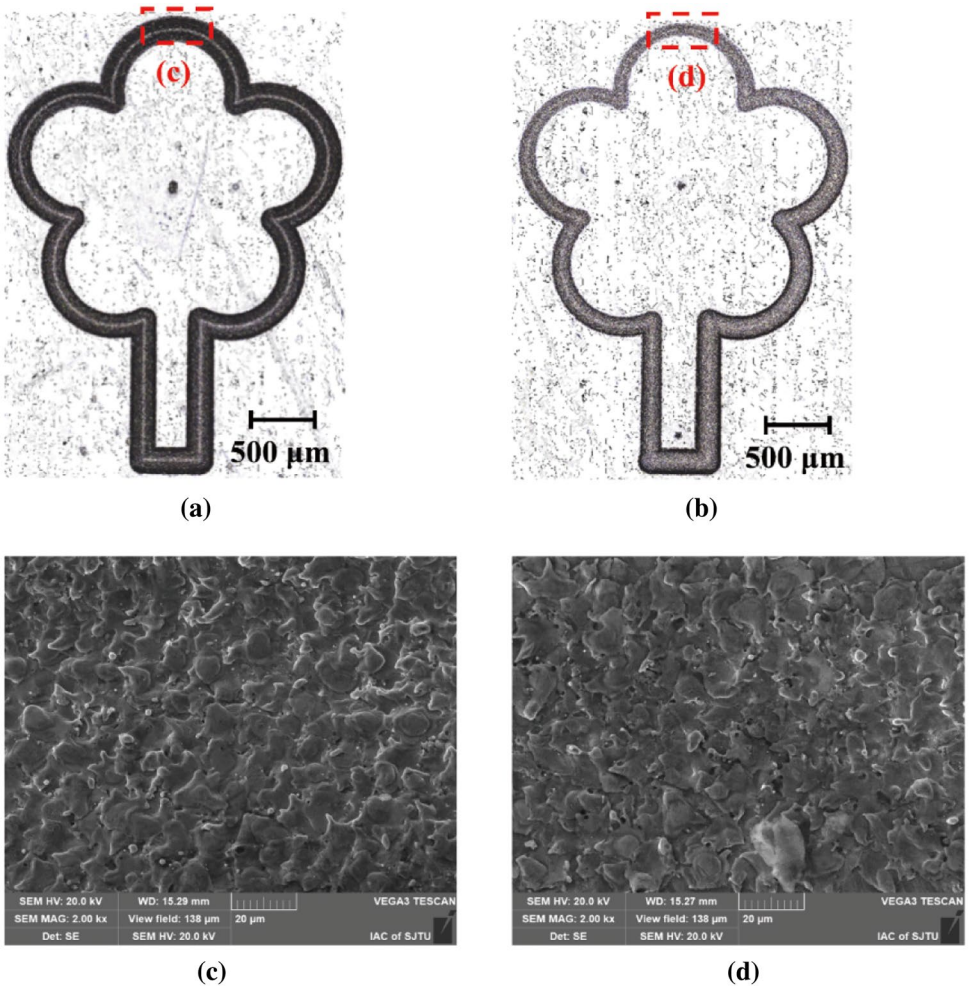

Fig. 17 Morphologies of a milled "flower" pattern **a** overall view of the pattern machined using the FPCC method, **b** overall view of the pattern machined using the 1TAV method, **c** local detail view of the red rectangle region in **a**, **d** local detail view of the red rectangle region in **b**

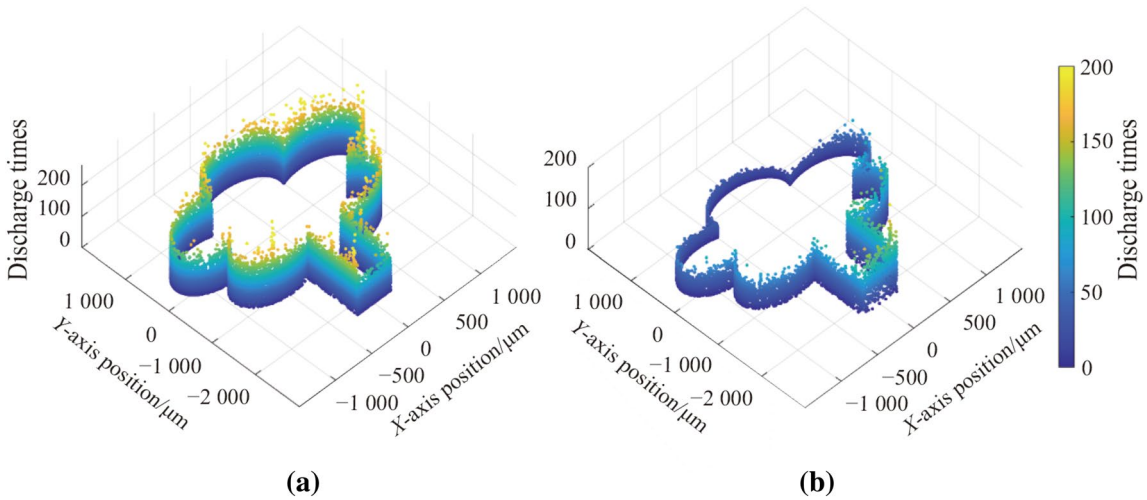

Fig. 18 Spatial distribution of discharge times during milling process **a** using FPCC method, and **b** using 1TAV method

Acknowledgements This work is financially supported by the National Natural Science Foundation of China (Grant Nos. 52175426, 52075333), National Science and Technology Major Projects of China (Grant No. 2018ZX04005001).

References

1. Tong H, Wang Y, Li Y (2008) Vibration-assisted servo scanning 3D micro EDM. J Micromech Microeng 18(2):025011. https://doi.org/10.1088/0960-1317/18/2/025011
2. Hashim NLS, Yahya A, Daud MR et al (2015) A review on electrical discharge machining servomechanism system. Sci Iran 22(5):1813–1832
3. Burek J, Babiarz R, Buk J et al (2021) The accuracy of finishing WEDM of inconel 718 turbine disc fir tree slots. Materials 14(3):562. https://doi.org/10.3390/ma14030562
4. Huang RN, Lou YJ, Chi GX (2010) Research on servo feeding system of micro WEDM. In: 2010 international conference on digital manufacturing and automation. IEEE, Changcha, 2010
5. Tong H, Liu X, Pu Y et al (2019) Servo control optimization of micro discharge gap and its reasonable matching with scanning speed in servo scanning 3D micro EDM based on threshold control method. Int J Adv Manuf Technol 105:3057–3066
6. Almeida S, Mo J, Bil C et al (2021) Comprehensive servo control strategies for flexible and high-efficient wire electric discharge machining. A systematic review. Precis Eng 71:7–28
7. Zhou M, Mu X, He L et al (2019) Improving EDM performance by adapting gap servo-voltage to machining state. J Manuf Process 37:101–113
8. Zhou M, Wu J, Xu X et al (2018) Significant improvements of electrical discharge machining performance by step-by-step updated adaptive control laws. Mech Syst Signal Process 101:480–497
9. Zhang L, Jia Z, Liu W et al (2012) A two-stage servo feed controller of micro-EDM based on interval type-2 fuzzy logic. Int J Adv Manuf Technol 59:633–645
10. Jahan MP, Wong YS, Rahman M (2009) A study on the quality micro-hole machining of tungsten carbide by micro-EDM process using transistor and RC-type pulse generator. J Mater Process Technol 209(4):1706–1716
11. Azhar WABW, Saleh T (2019) Development and performance evaluation of modular RC-based power supply for micro-EDM. In: 2019 7th international conference on mechatronics engineering (ICOM), IEEE, Putrajaya, 2019
12. Jahan MP, Wong YS, Rahman M (2008) A comparative study of transistor and RC pulse generators for micro-EDM of tungsten carbide. Int J Precis Eng Manuf 9(4):3–10
13. Hu MH, Li Y, Tong H (2010) Design and experimental study of a multi-mode controllable RC pulse generator for micro-EDM. In: international conference on advanced technology of design and manufacture (ATDM 2010), IET, Beijing, 2010
14. Abhilash PM, Chakradhar D (2021) Failure detection and control for wire EDM process using multiple sensors. CIRP J Manuf Sci Technol 33:315–326
15. Yan MT, Chien HT (2007) Monitoring and control of the micro wire-EDM process. Int J Mach Tools Manuf 47(1):148–157
16. Kumar D, Singh NK, Bajpai V (2020) Recent trends, opportunities and other aspects of micro-EDM for advanced manufacturing: a comprehensive review. J Braz Soc Mech Sci 42(5):222. https://doi.org/10.1007/s40430-020-02296-4
17. Han F, Wachi S, Kunieda M (2004) Improvement of machining characteristics of micro-EDM using transistor type isopulse generator and servo feed control. Precis Eng 28(4):378–385
18. Fu X, Zhang Q, Gao L et al (2016) A novel micro-EDM—piezoelectric self-adaptive micro-EDM. Int J Adv Manuf Technol 85:817–824
19. Lee WM, Liao YS (2007) Adaptive control of the WEDM process using a self-tuning fuzzy logic algorithm with grey prediction. Int J Adv Manuf Technol 34:527–537
20. Zhang Z, Ming W, Zhang G et al (2015) A new method for online monitoring discharge pulse in WEDM-MS process. Int J Adv Manuf Technol 81(5):1403–1418
21. Yeo SH, Aligiri E, Tan PC et al (2009) A new pulse discriminating system for micro-EDM. Mater Manuf Process 24(12):1297–1305
22. Liao YS, Woo JC (1997) The effects of machining settings on the behavior of pulse trains in the WEDM process. J Mater Process Technol 71(3):433–439
23. Muthuramalingam T, Mohan B, Rajadurai A et al (2013) Experimental investigation of iso energy pulse generator on performance measures in EDM. Mater Manuf Process 28(10):1137–1142
24. Tong H, Li Y, Wang Y et al (2008) Servo scanning 3D micro-EDM based on macro/micro-dual-feed spindle. Int J Mach Tools Manuf 48(7/8):858–869
25. Lim HS, Wong YS, Rahman M et al (2003) A study on the machining of high-aspect ratio micro-structures using micro-EDM. J Mater Process Technol 140(1/3):318–325

Qiang Gao is currently pursuing a doctoral degree in the Discipline of Mechanical Engineering at School of Mechanical Engineering, Shanghai Jiao Tong University, Shanghai, China. He has completed a B.S. degree in Mechanical Engineering from Jilin University, Changchun, China. His areas of interests are electrical discharging machining, pulse power supply for EDM, and adaptive servo control technology.

Ya-Ou Zhang is currently working as an assistant professor in the Discipline of Mechanical Engineering at School of Mechanical Engineering, Shanghai Jiao Tong University, Shanghai, China. He received the M.S. degree from Nanjing University of Aeronautics and Astronautics in 2003 and Ph.D. degree from Shanghai Jiao Tong University in 2008. His areas of interests are electrical discharging machining, specialized robot, and smart manufacturing.

Xue-Cheng Xi is currently working as an assistant professor in the Discipline of Mechanical Engineering at School of Mechanical Engineering, Shanghai Jiao Tong University, Shanghai, China. He received the M.S. and Ph.D. degrees in Automatic Control and Mechatronics from the National University of Singapore, Singapore, in 2003 and 2008. His areas of interests are electrical discharging machining, process and motion control, CNC systems, and artificial intelligence in manufacturing. He has contributed to more than forty publications in international journals/conference proceedings.

Yuan-Ding Wang is currently working as a senior engineer in the shanghai Institute of Space Propulsion, Shanghai, China. He received the B.S. and Ph.D. degrees from Nanjing University of Science and Technology (NUST) in 2010 and 2016. His research interests include advanced space propulsion technologies and application of electric discharge technology in space propulsion system.

Xiao-Fei Chen is currently working as a senior engineer in shanghai Institute of Space Propulsion, Shanghai, China. She received the M.S. degree from Harbin Institute of Technology in 2010. Her areas of interests are electrical discharging machining, machining process for production and special structure.

Wan-Sheng Zhao is currently working as a professor in the Discipline of Mechanical Engineering at School of Mechanical Engineering, Shanghai Jiao Tong University, Shanghai, China. He received the B.S., M.S. and Ph.D. degrees in Mechanical Engineering from Harbin Institute of Technology in 1982, 1984, and 1989. His research interests include electrical discharging machining, CNC systems for EDM machines towards smart manufacturing, and artificial intelligence in manufacturing.